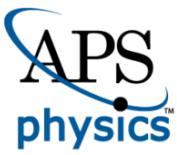

Ultrabroadband Entangled Photons on a Nanophotonic Chip

Usman A. Javid, Jingwei Ling, Jeremy Staffa, Mingxiao Li, Yang He, and Qiang Lin

Phys. Rev. Lett. **127**, 183601 — Published 27 October 2021

DOI: 10.1103/PhysRevLett.127.183601

Ultra-broadband Entangled Photons on a Nanophotonic Chip

Usman A. Javid[1,↑], Jingwei Ling[2,↑], Jeremy Staffa[1], Mingxiao Li[2], Yang He[2], and Qiang Lin[1,2*]
[1] *Institute Of Optics, University of Rochester, Rochester NY 14627, USA*
[2] *Department of Electrical and Computer Engineering, University of Rochester, Rochester NY 14627, USA and*
[↑] *These authors contributed equally.*
(Dated: August 3, 2021)

Development of quantum technologies on nanophotonic platforms have seem momentous progress in the past decade. Despite that, a demonstration of time-frequency entanglement over a broad spectral width is still lacking. Here we present an efficient source of ultra-broadband entangled photon pairs on a periodically poled lithium niobate nanophotonic waveguide. Employing dispersion engineering, we demonstrate a record-high 100 THz (1.2 um 2 um) generation bandwidth with a high efficiency of 13 GHz/mW and excellent noise performance with the coincidence-to-accidental ratio exceeding 10^5. We also measure strong time-frequency entanglement with over 98% two-photon interference visibility.

Introduction – Photonic quantum entanglement plays a central role in the functioning of a wide variety of applications including secure communication, metrology and sensing, and advanced computing [1]. Due to this, significant efforts have been devoted in the past decade in developing entangled photons on a variety of chip-scale platforms [2, 3] which allow flexible engineering of the properties of the emitted photons as well as significant improvement in the scalability and resource requirements for complex functionalities. A key aspect of this flexibility is the control of the dispersion of the optical modes guided on these chips. This becomes particularly useful in generating time-frequency entanglement over a broad spectral range and ultra-short coherence times. Broadband quantum entanglement adds significant advantages to quantum photonic applications, such as enhancing sensitivity and/or resolution in metrology [4], lithography [5], spectroscopy [6], nonlinear microscopy [7], quantum optical coherence tomography [8], clocking [9, 10], among many others. It also allows for wavelength-multiplexing protocols [11] as well as higher dimensional encoding of information [12, 13] to establish quantum networks for information processing and communication. However, the chip-scale photon sources developed so far exhibit fairly limited bandwidths, generally in the order of 100 GHz to a few THz (see for example [2, 3, 14–16]). A chip-scale demonstration of broadband photon pairs with temporal coherence approaching an optical cycle is yet to be seen. To date, broadband entangled photons are only available in bulk devices where a large bandwidth is obtained typically by a certain spatial modulation of the phase-matching condition, such as chirping the nonlinear grating [17–19], cascading nonlinear crystals [20], and spatially modulating the device temperature [21]. All these approaches, however, come at a cost of sacrificing the generation efficiency since different frequency components are produced only in different small sections of the device. In addition, the generated photons may not be transform-limited, requiring correction of the spectral phase. This trade-off of lower efficiency for bandwidth is inherently due to the inability to control dispersion in bulk materials.

In this article, we demonstrate generation of bright ultra-broadband entangled photon pairs on a nanophotonic chip using spontaneous parametric down-conversion (SPDC) on a dispersion-engineered thin-film lithium niobate (LN) waveguide as shown in Fig. 1(a) and (b). We demonstrate photon pair generation over a 100 THz bandwidth (1.2 μm – 2 μm), an order of magnitude larger than a typical chip-scale photon pair source and several times larger the ones with the widest spectrum [2, 3, 26, 33, 35]. We obtain a generation efficiency of 13 GHz/mW which is among the highest ever reported for a broadband entangled photon pair source [17–20, 22–24, 27, 33, 35–37], an unprecedented coincidence-to-accidental ratio (CAR) of 150,000 within a 17 nm wide spectral region in the telecom band, and a visibility of 98.8% for Franson-type quantum interference. This first nanophotonic demonstration of entanglement over hundreds of nanometers of bandwidth rivals its most well-established and optimized bulk counterparts in performance.

Biphoton spectrum – The bandwidth of SPDC process relies critically on the phase-matching among the interacting modes which is dominated by the group velocity dispersion (GVD) and higher even-order dispersion parameters (see supplementary materials for details [38]). Therefore, we utilize the waveguide geometry to engineer these parameters to be very close to zero at the center of the SDPC spectrum to obtain a broad phase-matching bandwidth as shown in Fig. 1(d)-(f), with the fabricated waveguide's width set at 1450 nm. The bandwidth of the generated photons is measured directly with an infrared spectrometer. In this measurement, we scan the pump laser wavelength around 775 nm to evaluate the SPDC bandwidth dependence on pump detuning. For the rest of the article, we will refer to the wavelengths shorter/longer than the spectral-center wavelength as sig-

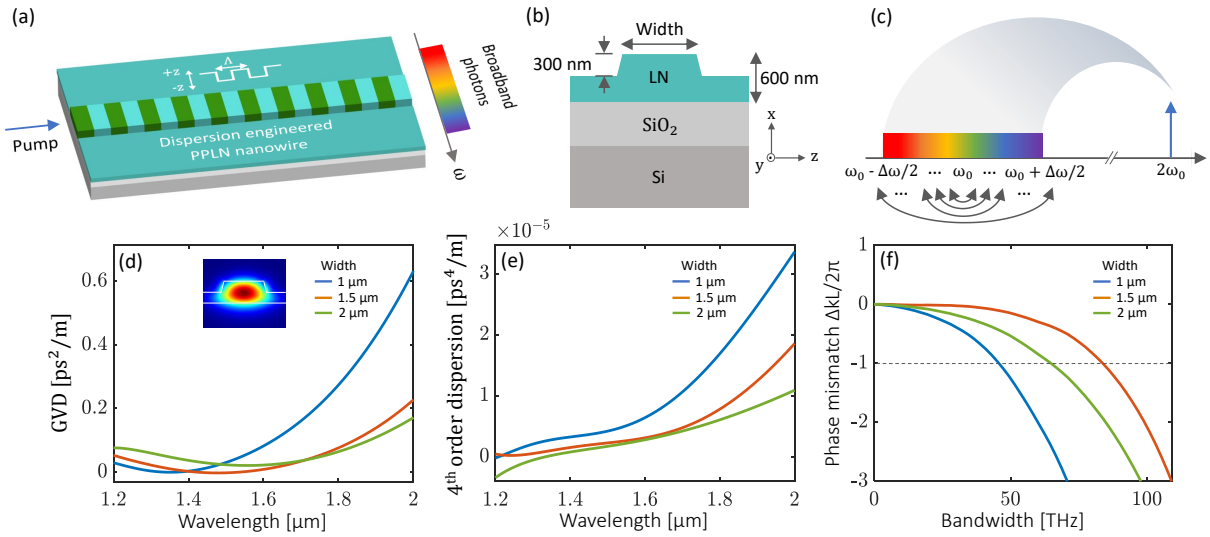

FIG. 1. (a) A periodically poled thin-film lithium niobate waveguide with its cross-section shown in (b). The device generates a broadband SPDC spectrum with pump at frequency $2\omega_0$ creating two photons with frequencies equally spaced around the center frequency ω_0. Controlling dispersion with waveguide width with variations in the group velocity dispersion plotted in (d) and the fourth-order dispersion in (e). The inset in (d) shows a cross-section of the waveguide with the fundamental quasi-TE mode at 1550 nm. (f) the phase-mismatch ΔkL, where k is the wavevector, is plotted for a waveguide length L = 5 mm with an appropriate choice of poling period. Dashed line indicates the first zero of the phase-mismatch Sinc function.

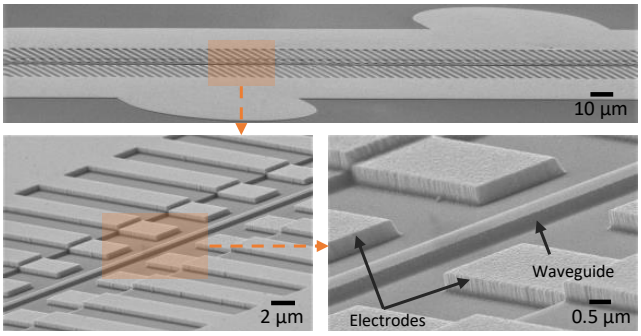

FIG. 2. Scanning electron microscope (SEM) images of a fabricated device at different magnifications.

nal/idler. At a pump wavelength of 770.4 nm, we obtain a spectrum with the largest bandwidth plotted in Fig. 3(a). Here we measure a degenerate SPDC spectrum stretching down to 1200 nm with a 1540.8 nm center wavelength and a 50 THz 3-dB half-bandwidth. The spectrum extends up to the 1590 nm after which the spectrometer's InGaAs CCD cuts off any further measurement at idler wavelengths. Therefore we rely on the signal spectrum to get the bandwidth. Energy conservation dictates that the spectral width of the generated photons should be symmetric around the pump half-frequency. This gives a 100 THz (800 nm) total biphoton bandwidth with the idler spectrum expected to span up to 2 μm in the mid-IR region. To the best of our knowledge, this is the largest SPDC spectral width on any nanophotonic de-

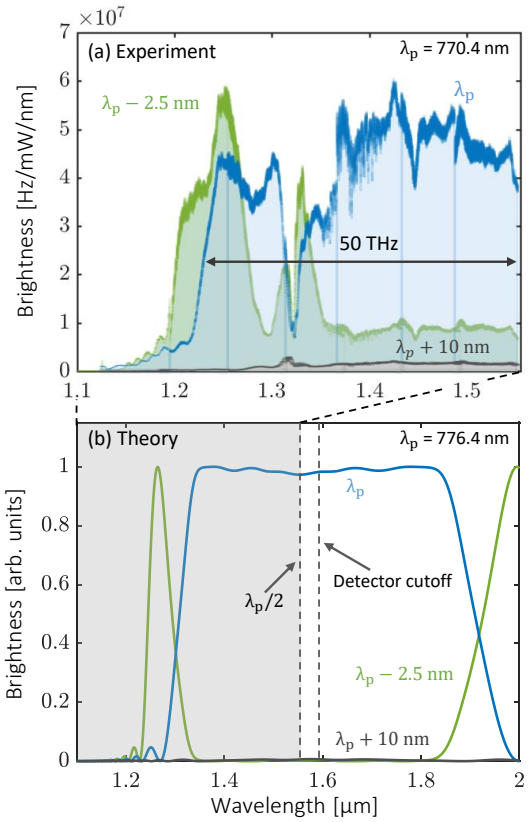

FIG. 3. (a) Signal spectrum at different pump wavelengths with λ_p corresponding to the pump wavelength that gives the widest spectrum. (b) The corresponding simulated plots for the designed waveguide.

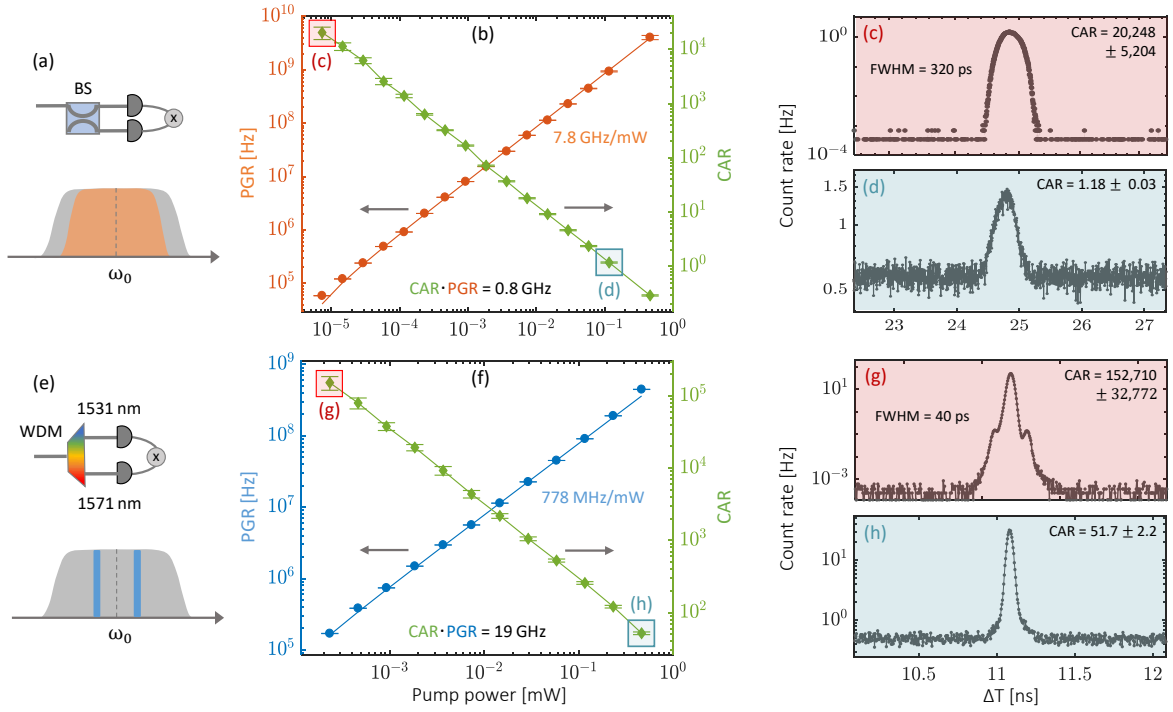

FIG. 4. (a) Coincidence measurements for the full spectrum. (b) Pair generation rates and CAR measurement for the photon pairs for increasing pump powers with linear fits. (c) and (d) Coincidence histograms for two points indicated in (b) with the corresponding CAR values. (e)-(h) Similar measurements done with the spectrum filtered at 1531 nm and 1571 nm using a wavelength-division multiplexer (WDM). ΔT: difference in arrival times of the two photons, BS: beam splitter.

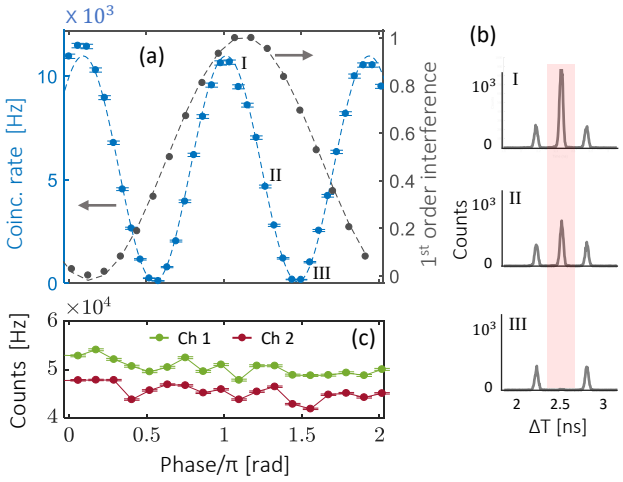

FIG. 5. (a) Two-photon interferogram with sinusoidal fit, along with first-order interference with a laser at a similar wavelength as the photons. (b) Sample coincidence histograms versus signal-idler delay ΔT at three points indicated in (a). (c) The corresponding singles counts at the two detectors indicating no first-order interference in the photon pairs.

vice [2, 3, 33, 35, 39]. Integrating the spectrum, we get a total on-chip efficiency of 13 GHz/mW of pump power. When the pump is blue-detuned by 2.5 nm, we find a second phase-matching point. Here the photons are strongly non-degenerate in frequency with the signal spectrum peaked at 1250 nm with a ∼ 70 nm width and the idler is expected to be at 2000 nm. The corresponding theory plots in Fig. 3(b) show good qualitative agreement with an ∼ 80 THz bandwidth which was also indicated in the phase-mismatch calculation in Fig. 1(f) (see supplementary materials [38] for a note on discrepancies between theory and experiment).

Temporal correlations – We characterize the temporal correlations of the generated photons by separating them using a 50:50 fiber beam splitter and using standard coincidence counting to obtain a histogram of differences in arrival times of the two photons. The pair generation rate (PGR) is plotted for increasing pump power in Fig. 4(b). The data fits cleanly to a straight line and we obtain an on-chip efficiency of 7.8 GHz/mW. This efficiency is limited by the detection bandwidth as we obtained roughly twice as high efficiency with the spectrometer. In order to measure the noise characteristics of the source, we evaluate the coincidence-to-accidental ratio (CAR). The results are plotted in green in Fig. 4(b). The highest CAR obtained in this experiment is 20,248 ± 5,204 at a PGR of 52 ± 0.4 KHz (see supplementary materials [38] for details on the measurement uncertainties), and decreases with increasing PGR due to a higher rate of multi-pair generation events. Although this value is quite high, due to the broad spectrum, the highest achievable

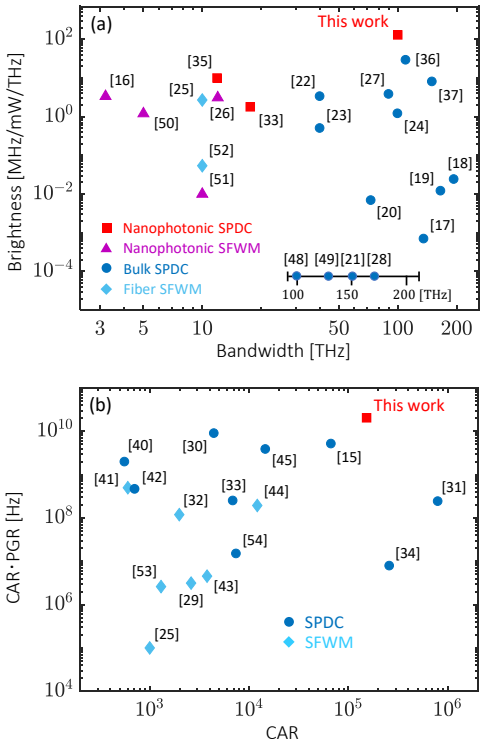

FIG. 6. (a) Bandwidth and brightness for some recent demonstrations of broadband SPDC and SFWM. Inset at the bottom shows references for which brightness is not available. Brightness was evaluated from reported photon flux, input power and number of modes in [22], from reported photon flux, and laser power in [23, 24], from ratio of singles flux to coincidence flux and reported laser power in [19, 20], from plotted photon flux, filter width and input power in [18, 25], from laser pulse width and peak power, photons per pulse and DWDM channel width in [26]. Bandwidth was extracted from plotted spectrum in [17, 23, 24, 27, 28] and WDM bandwidth in [16]. (b) Maximum CAR and CAR PGR product for for some recent demonstrations of SFWM and SPDC. PGR was evaluated from stated coincidence rate in [25], from photon pairs per pulse and laser repetition rate in [29–31], from stated brightness, bandwidth and input power in [32, 33], extracted from PGR plot in [34].

CAR is being limited by the dispersion in the experimental setup. This includes asymmetric wavelength dependence of the detectors' quantum efficiency, and dispersion in the beam splitter and the optical fibers. This can be seen in the coincidence histograms in Fig. 4(c),(d) which have a dispersion-broadened full-width at half-maximum (FWHM) of 320 ps, much larger that the 40 ps timing jitter of the detection system.

To demonstrate the true noise characteristics of the generated photons, we filter the signal and idler photons into two 17 nm channels centered at 1531 nm (signal) and 1571 nm (idler) using a wavelength-division multiplexer (WDM). The signal and idler photons are roughly equally spaced from the spectral center when pumped at 775 nm. This removes all wavelength-dependent effects in the measurement. The results are shown in Fig. 4(f)-(h). We clearly see in the coincidence histogram in Fig. 4(g), (h) that the FWHM now shrinks to 40 ps, matching with the timing jitter of the detectors. For this measurement, we obtain a generation efficiency of 778 MHz/mW and a brightness of 38 MHz/mW/nm which is in good agreement with the 43 MHz/mW/nm brightness obtained with the spectrometer in Fig. 3(a). We obtain our highest CAR of 152,710 ± 32,772 at a PGR of 176 ± 0.7 KHz. To the best of our knowledge, this is the highest CAR obtained on a chip-scale device [15, 29, 30, 32, 33, 40–45]. An even higher CAR can actually be obtained using smaller pump powers and integrating for longer periods of time [31], ultimately limited by dark counts of the photodetectors for SPDC sources. The highest CAR was obtained at a signal-to-noise ratio of 20 between the photon flux and dark counts at the detectors indicating that we can go further. A better estimate of the noise characteristics of a photon pair source is the product of CAR and PGR which evaluates device performance independently of the dark counts and pump power in the experiment. The product of CAR and PGR evaluates to 19 GHz and 0.8 GHz for the filtered and full spectrum respectively, indicating low noise even at high rates of photon emission. We further verify the non-classical behavior of the generated light, using a two-photon interference measurement. The time-energy entanglement present in SPDC can be verified using a Bell's inequality violation [46] by beating a 70.7% visibility limit in two-photon interference. For this, we run an interference experiment in a folded Michelson interferometer [47] on the filtered signal and idler photons (see supplementary materials for details [38]). Figure 5(a) shows the results of the measurement. The interference data is fitted to a sinusoid giving a visibility of 98.8%, violating the Bell's inequality. This measurement was not done for the full spectrum due to its large bandwidth which will cause significant experimental challenges such as dispersion in the interferometer and the optical fibers which will artificially reduce the visibility, and the absence of filters that can be tuned over the 800 nm bandwidth. We expect similar performance for the rest of the spectrum.

Discussion – In Fig. 6(a), we compare the bandwidth and efficiency of some of the state-of-the art broadband SPDC sources to our device. Most of these sources are bulk crystals and waveguides carved into bulk wafers since there has not been much work done on nanophotonic SPDC sources for bandwidth. The plot clearly demonstrates the superior efficiency of our device. Some of these experiments do not report the device efficiency since that may not be their primary concern. We reference these results [21, 28, 48, 49] in the inset of Fig. 6(a). We also include results obtained with spontaneous four-wave mixing (SFWM) in semiconductor waveguides and optical fibers [16, 25, 26, 50–52] with the brightness evaluated at a pump power of 1 mW since SFWM is a third

order nonlinear process with a photon flux quadratic with pump power. The comparison demonstrates that waveguide dispersion can greatly enhance bandwidth of photon pairs in SPDC rather effortlessly as indicated by the stark difference in bandwidth demonstrated in our work to previous chip-scale devices. In Figure 6(b) we plot the product of maximum CAR and PGR for a few recent experiments in photon pair generation that have reported among the highest CAR values (> 500) [15, 25, 29–32, 34, 40–45, 53, 54]. Our device gives among the highest reported CAR $\cdot$ PGR product, noting that much higher CAR values have been reported albeit at much lower coincidence rates [31, 34].

To summarize, we have presented a broadband photon pair source based on thin-film lithium niobate with a record-high 100 THz bandwidth spanning near- and mid-IR spectral regions and a high generation efficiency of 13 GHz/mW. Time domain measurements show coincidence-to-accidental ratio exceeding 10^5 and a near-unity quantum interference visibility. These qualities make a strong case for nanophotonic LN devices as good sources for wavelength-multiplexed quantum communication and and entanglement distribution. Furthermore, we envision that this work will motivate efforts to bring femtosecond metrology, spectroscopy and nonlinear microscopy to nanophotonic platforms.

This work is supported in part by National Science Foundation (NSF) (EFMA-1641099, ECCS-1810169, and ECCS-1842691); the Defense Threat Reduction Agency-Joint Science and Technology Office for Chemical and Biological Defense (grant No. HDTRA11810047); and the Defense Advanced Research Projects Agency (DARPA) under Agreement No. HR00112090012. This work was performed in part at the Cornell NanoScale Facility, a member of the National Nanotechnology Coordinated Infrastructure (NNCI), which is supported by the National Science Foundation (Grant NNCI-2025233).

* qiang.lin@rochester.edu

[1] J. Wang, F. Sciarrino, A. Laing, and M. G. Thompson, Nature Photonics **14**, 273 (2020).
[2] G. Moody, L. Chang, T. J. Steiner, and J. E. Bowers, AVS Quantum Science **2**, 041702 (2020).
[3] L. Caspani, C. Xiong, B. J. Eggleton, D. Bajoni, M. Liscidini, M. Galli, R. Morandotti, and D. J. Moss, Light: Science & Applications **6**, e17100 (2017).
[4] V. Giovannetti, S. Lloyd, and L. Maccone, Nature photonics **5**, 222 (2011).
[5] A. N. Boto, P. Kok, D. S. Abrams, S. L. Braunstein, C. P. Williams, and J. P. Dowling, Physical Review Letters **85**, 2733 (2000).
[6] B. E. Saleh, B. M. Jost, H.-B. Fei, and M. C. Teich, Physical review letters **80**, 3483 (1998).
[7] B. Dayan, A. Pe'er, A. A. Friesem, and Y. Silberberg, Physical review letters **93**, 023005 (2004).
[8] A. F. Abouraddy, M. B. Nasr, B. E. Saleh, A. V. Sergienko, and M. C. Teich, Physical Review A **65**, 053817 (2002).
[9] V. Giovannetti, S. Lloyd, and L. Maccone, Nature **412**, 417 (2001).
[10] A. Valencia, G. Scarcelli, and Y. Shih, Applied Physics Letters **85**, 2655 (2004).
[11] H. C. Lim, A. Yoshizawa, H. Tsuchida, and K. Kikuchi, Optics express **16**, 22099 (2008).
[12] B. Bessire, C. Bernhard, T. Feurer, and A. Stefanov, New journal of physics **16**, 033017 (2014).
[13] J. Roslund, R. M. De Araujo, S. Jiang, C. Fabre, and N. Treps, Nature Photonics **8**, 109 (2014).
[14] H. Jin, F. Liu, P. Xu, J. Xia, M. Zhong, Y. Yuan, J. Zhou, Y. Gong, W. Wang, and S. Zhu, Physical review letters **113**, 103601 (2014).
[15] J. Zhao, C. Ma, M. Rüsing, and S. Mookherjea, Physical Review Letters **124**, 163603 (2020).
[16] Y.-H. Li, Z.-Y. Zhou, L.-T. Feng, W.-T. Fang, S.-l. Liu, S.-K. Liu, K. Wang, X.-F. Ren, D.-S. Ding, L.-X. Xu, *et al.*, Physical Review Applied **7**, 064005 (2017).
[17] M. B. Nasr, S. Carrasco, B. E. Saleh, A. V. Sergienko, M. C. Teich, J. P. Torres, L. Torner, D. S. Hum, and M. M. Fejer, Physical review letters **100**, 183601 (2008).
[18] A. Tanaka, R. Okamoto, H. H. Lim, S. Subashchandran, M. Okano, L. Zhang, L. Kang, J. Chen, P. Wu, T. Hirohata, *et al.*, Optics express **20**, 25228 (2012).
[19] M. Okano, H. H. Lim, R. Okamoto, N. Nishizawa, S. Kurimura, and S. Takeuchi, Scientific reports **5**, 18042 (2015).
[20] M. Okano, R. Okamoto, A. Tanaka, S. Subashchandran, and S. Takeuchi, Optics Express **20**, 13977 (2012).
[21] K. Katamadze and S. Kulik, Journal of Experimental and Theoretical Physics **112**, 20 (2011).
[22] M. V. Chekhova, S. Germanskiy, D. B. Horoshko, G. K. Kitaeva, M. I. Kolobov, G. Leuchs, C. R. Phillips, and P. A. Prudkovskii, Optics letters **43**, 375 (2018).
[23] S. Sensarn, G. Yin, and S. Harris, Physical review letters **104**, 253602 (2010).
[24] Y. Shaked, R. Pomerantz, R. Z. Vered, and A. Pe'er, New Journal of Physics **16**, 053012 (2014).
[25] J. Fan and A. Migdall, Optics express **15**, 2915 (2007).
[26] K.-i. Harada, H. Takesue, H. Fukuda, T. Tsuchizawa, T. Watanabe, K. Yamada, Y. Tokura, and S.-i. Itabashi, IEEE Journal of Selected Topics in Quantum Electronics **16**, 325 (2009).
[27] K. A. O'Donnell and A. B. U'Ren, Optics letters **32**, 817 (2007).
[28] N. Mohan, O. Minaeva, G. N. Goltsman, M. F. Saleh, M. B. Nasr, A. V. Sergienko, B. E. Saleh, and M. C. Teich, Applied optics **48**, 4009 (2009).
[29] X. Lu, S. Rogers, T. Gerrits, W. C. Jiang, S. W. Nam, and Q. Lin, Optica **3**, 1331 (2016).
[30] Q. Zhang, X. Xie, H. Takesue, S. W. Nam, C. Langrock, M. Fejer, and Y. Yamamoto, Optics express **15**, 10288 (2007).
[31] T. Inagaki, N. Matsuda, O. Tadanaga, M. Asobe, and H. Takesue, Optics express **21**, 23241 (2013).
[32] J. A. Steidle, M. L. Fanto, C. C. Tison, Z. Wang, S. F. Preble, and P. M. Alsing, in *Quantum Information and Computation XIII*, Vol. 9500 (International Society for Optics and Photonics, 2015) p. 950015.
[33] B. S. Elkus, K. Abdelsalam, A. Rao, V. Velev, S. Fathpour, P. Kumar, and G. S. Kanter, Optics Express **27**,

38521 (2019).
[34] M. Bock, A. Lenhard, C. Chunnilall, and C. Becher, Optics express **24**, 23992 (2016).
[35] D. Kang, A. Anirban, and A. S. Helmy, Optics express **24**, 15160 (2016).
[36] B. Cao, R. Okamoto, M. Hisamitsu, K. Tokuda, and S. Takeuchi, in *European Quantum Electronics Conference* (Optical Society of America, 2019) p. eb_p_25.
[37] B. Cao, K. Hayama, M. Hisamitsu, K. Tokuda, S. Kurimura, R. Okamoto, and S. Takeuchi, in *CLEO: Science and Innovations* (Optical Society of America, 2020) pp. STh4G–4.
[38] See Supplemental Material at [URL will be inserted by publisher] for details.
[39] R. Luo, H. Jiang, S. Rogers, H. Liang, Y. He, and Q. Lin, Optics express **25**, 24531 (2017).
[40] X. Guo, C.-l. Zou, C. Schuck, H. Jung, R. Cheng, and H. X. Tang, Light: Science & Applications **6**, e16249 (2017).
[41] E. Engin, D. Bonneau, C. M. Natarajan, A. S. Clark, M. G. Tanner, R. H. Hadfield, S. N. Dorenbos, V. Zwiller, K. Ohira, N. Suzuki, *et al.*, Optics express **21**, 27826 (2013).
[42] J.-y. Chen, Y. M. Sua, Z.-h. Ma, C. Tang, Z. Li, and Y.-p. Huang, OSA Continuum **2**, 2914 (2019).
[43] X. Lu, Q. Li, D. A. Westly, G. Moille, A. Singh, V. Anant, and K. Srinivasan, Nature physics **15**, 373 (2019).
[44] C. Ma, X. Wang, V. Anant, A. D. Beyer, M. D. Shaw, and S. Mookherjea, Optics Express **25**, 32995 (2017).
[45] Z. Ma, J.-Y. Chen, Z. Li, C. Tang, Y. M. Sua, H. Fan, and Y.-P. Huang, Physical Review Letters **125**, 263602 (2020).
[46] J. D. Franson, Physical review letters **62**, 2205 (1989).
[47] J. Brendel, E. Mohler, and W. Martienssen, Physical review letters **66**, 1142 (1991).
[48] K. Katamadze, N. Borshchevskaya, I. Dyakonov, A. Paterova, and S. Kulik, Physical Review A **92**, 023812 (2015).
[49] M. Okano, H. H. Lim, R. Okamoto, A. Tanaka, Y. Nagamatsu, N. Nishizawa, S. Kurimura, and S. Takeuchi, in *Frontiers in Optics* (Optical Society of America, 2014) pp. FW1C–4.
[50] S. Clemmen, K. P. Huy, W. Bogaerts, R. G. Baets, P. Emplit, and S. Massar, Optics express **17**, 16558 (2009).
[51] P. Kultavewuti, E. Y. Zhu, L. Qian, V. Pusino, M. Sorel, and J. S. Aitchison, Optics express **24**, 3365 (2016).
[52] J. Fan, M. Eisaman, and A. Migdall, Physical Review A **76**, 043836 (2007).
[53] S. D. Dyer, M. J. Stevens, B. Baek, and S. W. Nam, Optics express **16**, 9966 (2008).
[54] S. Krapick, H. Herrmann, V. Quiring, B. Brecht, H. Suche, and C. Silberhorn, New Journal of Physics **15**, 033010 (2013).